Baghdad Science Journal

Volume 23 | Issue 4 Article 3

4-20-2026

Raman Spectroscopy and Optical Properties of CeO_2:Al_2O_3 Nanocomposites Synthesized by Pulsed Laser Deposition

Alaa Nazar Abd Algaffar
Department of Physics, College of Sciences for Women, University of Baghdad, Baghdad, Iraq,
alaana_phys@csw.uobaghdad.edu.iq

Noha H. Harb
Department of Physics, College of Sciences for Women, University of Baghdad, Baghdad, Iraq,
noha.Harb1104@sc.uobaghdad.edu.iq

Sabah N. Mazhir
Department of Physics, College of Sciences for Women, University of Baghdad, Baghdad, Iraq,
sabahnm_phys@csw.uobaghdad.edu.iq

How to Cite this Article

Algaffar, Alaa Nazar Abd; Harb, Noha H.; and Mazhir, Sabah N. (2026) "Raman Spectroscopy and Optical Properties of CeO_2:Al_2O_3 Nanocomposites Synthesized by Pulsed Laser Deposition," *Baghdad Science Journal*: Vol. 23: Iss. 4, Article 3.
DOI: https://doi.org/10.21123/2411-7986.5257

BAGHDAD SCIENCE JOURNAL 2026;23(4):1135–1145

Scan the QR to view the full-text article on the journal website

RESEARCH ARTICLE

Raman Spectroscopy and Optical Properties of CeO_2:Al_2O_3 Nanocomposites Synthesized by Pulsed Laser Deposition

Alaa Nazar Abd Algaffar *, Noha H. Harb, Sabah N. Mazhir

Department of Physics, College of Sciences for Women, University of Baghdad, Baghdad, Iraq

ABSTRACT

This study investigated the effects of laser energy on the phase-change mechanism, optical properties, and structure of CeO_2:Al_2O_3 nanoparticles synthesized via pulsed laser deposition (PLD). The study employed Raman spectroscopy, UV-Vis spectroscopy, X-ray diffraction (XRD), atomic force microscopy (AFM), and field emission scanning electron microscopy (FESEM). The process techniques were compared at different laser pulse intensities (530, 730, and 930 mJ). Porous silicon (PS) substrates have been created using the photoelectrochemical etching of n-type silicon. The XRD results for CeO_2:Al_2O_3 nanoparticles indicated a polycrystalline cubic phase. Raman spectroscopy of CeO_2:Al_2O_3 revealed weak peaks at around 615 and 1311 cm^{-1} and major peaks at approximately 452, 519, and 979 cm^{-1}, with their intensities increasing with laser energy. The RMS surface roughness increases with increasing laser energy. The majority of nanocomposites feature spherical nanostructures that are randomly distributed and increase in size with increasing laser power. The optical bandgap of CeO_2:Al_2O_3 thin films was determined to be 2.36, 2.62, and 2.66 eV for the varying laser energies. The quantum confinement effect caused the energy gap to widen as the laser pulse energy grew. Cerium oxide significantly contributes to the results and is chosen over traditional materials in nanocomposites because it enhances the properties of the base materials and makes them more stable when deposited at high temperatures, as observed in this work. It is also used in optical applications and a variety of other applications.

Keywords: CeO_2:Al_2O_3 composite, Optical properties, Pulse laser deposition, Photo electrochemical etching, Raman

Introduction

Two materials with dissimilar chemical and physical Characteristics are combined to create a composite. When these constituent materials, which differ significantly in their chemical or physical characteristics, combine, a material is produced that possesses unique properties.[1,2] Composites are distinguished from mixes and solid solutions by the fact that the constituent parts of the final structure remain distinct and independent.[3] The combination of these results in a material that is specialized to perform a given function, such as becoming stronger, lighter, or electrically resistant.[4] They can increase Stiffness and strength as well. Composite materials are employed in many aspects of our daily life, including building, medicine, oil and gas, sports, transportation, and aerospace. In recent Times, Scientists have also begun to actively incorporate communication, computing, actuation, and sensing into composites, often referred to as robotic materials.[5,6] Oxide thin films play a significant role in both present-day and future solid-state electronic devices. The unique chemistry of cerium oxide (CeO_2) nanoparticles makes them the most studied. CeO_2, sometimes called ceria, is an n-type semiconductor with exceptional chemical and electrical characteristics. Among these attributes are remarkable optical activity, sufficient

Received 28 April 2025; revised 18 July 2025; accepted 21 July 2025.
Available online 20 April 2026

* Corresponding author.
E-mail addresses: alaana_phys@csw.uobaghdad.edu.iq (A. N. Abd Algaffar), noha.harb1104@sc.uobaghdad.edu.iq (N. H. Harb), sabahnm_phys@csw.uobaghdad.edu.iq (S. N. Mazhir).

https://doi.org/10.21123/2411-7986.5257

surface area, strong chemical stability, photocatalytic activity, and electrochemical activity.[7–9] Cerium oxide is commonly used in industrial catalysis for several purposes, such as fixing carbon dioxide, eliminating carbon monoxide, and producing hydrogen, among many other environmental uses.[10] The optical bandgap of CeO_2 is around 2.6–3.1 eV.[11] This is supported by CeO2's large surface area, crystallization potential, and most significantly, the creation of oxygen vacancies, which render it an effective photocatalyst.[12] Aluminum oxide (Al_2O_3) is a crucial ceramic substance used in microelectronic, optical, and structural applications. Several polymorphs of Al_2O_3 exist, including the γ, θ, κ, and α-phases.[13] The dielectric substance Al_2O_3 has a broad band-gap of 6 eV at 300 K for bulk material.[14] In several industrial applications, including gas diffusion barriers, sensors, anti-reflection coatings, catalysts, surface passivation, abrasive materials, optical interference filters, and nano laminates, nanostructured aluminum oxide is the most significant metal oxide material.[13–15] In comparison to the two pure individual oxides, the catalyst's characteristics are improved by the combination of CeO_2 and Al_2O_3. Most metal oxide-covered adsorbents are more effective than metal oxides alone, according to several studies. Different techniques have been used to create the CeO_2 and Al_2O_3 nanostructures, and metal oxide-coated absorbents are generally more effective than metal oxides alone.[16–20] In this study, CeO_2:Al_2O_3 NPs were synthesized via the pulsed laser deposition (PLD) method with different pulse laser energies of 530, 730, and 930 mJ, and their performance was studied. All the prepared materials were fully characterized using XRD, AFM, FESEM, Raman, and UV-vis spectroscopy techniques.

We studied the applicability of the pulsed laser deposition technique in producing CeO_2:Al_2O_3 composite nanoparticles with varying concentrations of each material, as well as the potential applications of these oxides in optical coatings. When CeO_2:Al_2O_3 is prepared on the PS surface, its photocatalytic performance may be effectively increased. Porous silicon has been demonstrated to be a desirable template for the PLD deposition of metal nanostructures. Metals are PLD-deposited not only at the bottom of pores but also on the pore wall and pore apertures because porous silicon is a semiconductive porous electrode.

Experimental

First, the 3×2 cm^2 glass slides were cleaned for 15 minutes with alcohol and ultrasonic waves to remove residues and impurities, as shown in Fig. 1(a). Next, a solution of hydrofluoric acid (HF, 48%) and ethanol (C_2H_5OH, 99.9%) was prepared for immersing the n-type silicon wafer. The wafer was then placed in

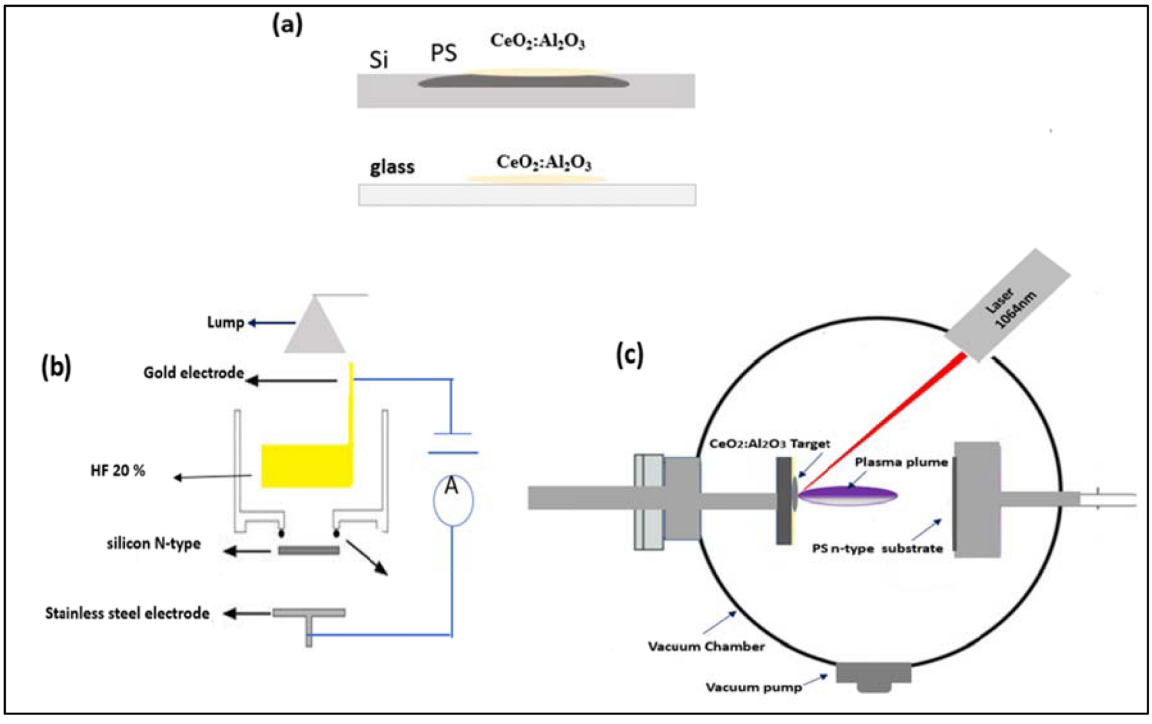

Fig. 1. Experimental setup devices: (a) CeO_2: Al_2O_3 deposition on substrate porous silicon and glass, (b) Photo electrochemical etching, and (c) Pulsed laser deposition.

the electrolyte containing 20% HF within a Teflon cell. Photoelectrochemical etching was performed by applying an anodic current of 24 mA/cm^2 for 15 minutes, using a silicon wafer as the anode and a gold electrode as the cathode, as shown in Fig. 1(b). The substrates were finally dried by blowing air over them. In order to prepare CeO_2: Al_2O_3 nanocomposite particles, PLD uses a Q-switched Nd: YAG laser with a wavelength of 1064 nm, a number of shots of 500, a repetition rate of 6 Hz, and energy pulses of 530, 730, and 930 mJ as shown in Fig. 1(c). A pulsed and concentrated laser beam strikes target material at an angle of 45° in a vacuum chamber up to 10^{-2} mbar. Cerium oxide powder and Aluminum oxide powder of high purity 99.999% have been mixed for 30 minutes at weight percentages of (CeO_2 5.5 % wt and Al_2O_3 4.5% wt) using an agate mortar. The mixing powder is next compressed using a hydraulic press to form pellets that are 1.5 cm in diameter and 3 cm thick, which were pressed under 5 tons. The structural properties of deposited thin films were investigated using the 2θ scan with Cu-kα at a wavelength 1.5406A° current of 30 mA. On the Miniflex X-ray diffraction (XRD), the scanning angle 2θ is adjusted between 10 and 75 degrees. The crystallite sizes were calculated using the Debye-Scherrer Eq. (1).[21]

$$D = \frac{0.94\lambda}{\beta \cos\theta} \tag{1}$$

Where D: the average size of the crystallites, θ: the diffraction peak's degree, and β: the peak width of the diffraction peak profile at half of the height that results from the tiny crystallite size in radians. We studied the optical properties of CeO_2: Al_2O_3 composite nanostructures in the 300–1200 nm range using UV-V is spectroscopy. The optical energy gap for the CeO_2: Al_2O_3 nanocomposite has been determined using Eq. (2).[22]

$$\alpha h\nu = B(h\nu - Eg)^r \tag{2}$$

Studying the refractive index and the extinction coefficient can be calculated using Eq. (3).[22]

$$n = \left(\frac{4R}{(R-1)^2} - k^2\right)^{\frac{1}{2}} - \frac{R+1}{R-1} \tag{3}$$

Where k: the extinction coefficient and R: the reflectance, as shown in the Eqs. (4) and (5) below.[22]

$$R = \frac{(n-1)^2 + k^2}{(n+1)^2 + k^2} \tag{4}$$

$$k = \frac{\alpha\lambda}{4\pi} \tag{5}$$

where: α: the absorption coefficient is calculated using Eq. (6).[21]

$$\alpha = 2.303\frac{A}{t} \tag{6}$$

where A: the absorbance and t: thickness

Results and discussion

X-Ray diffraction analysis of CeO_2:Al_2O_3 nanocomposite

The X-ray diffraction of CeO_2:Al_2O_3 thin film produced by PLD with different laser pulse energies 530, 730, and 930 mJ using a 1064 nm Nd: YAG laser on glass substrate is displayed in Fig. 2. The XRD at 530 and 730 mJ pulse laser energy showed two reflection peaks at two different amounts, 28° that correspond to the reflections of the cubic CeO_2 material (111) and the cubic Al_2O_3 material (400). When they were exposed to a 930 mJ high-energy pulse, they became polycrystalline. At angles of diffraction of 28°, 33°, 56°, and 76°, the crystalline levels of the CeO_2 material with peak numbers (111), (200), (311), and (420) are formed JCPDS file No. 34−0394 and lattice parameter was 5.44 Å,[19] whereas the reflections of the Al_2O_3 material are generated at angle 47° (400) JCPDS file No. 50-741 and lattice parameter was 7.90 Å,[23] suggests the presence of a very small amount of Al_2O_3. An XRD diffractogram of CeO_2:Al_2O_3 nanoparticles shows that the material was successfully prepared using PLD. When high laser pulse energy is supplied, higher mobility results from increased atom energy. Eventually, it results in the structure becoming more organized and recrystallizing. As the pulse strength of laser deposition increases, the CeO_2:Al_2O_3 XRD patterns get sharper and more intense. The crystallite sizes were calculated using Eq. (1). The FWHM, dhkl, and crystallite size are shown in Table 1 as the laser pulse intensity was increased. The FWHM decreased as the crystalline size increased.

Raman spectroscopy of CeO_2:Al_2O_3 nanocomposite

CeO_2:Al_2O_3 nanoparticle composition, structure, and phase characterization have all been thoroughly determined using the Raman spectroscopy method. The positions of the peaks in the measured Raman spectra of cerium oxide and Aluminum oxide structures nanocomposites deposited on PS n-type substrate are shown in Fig. 3. Similar spectral patterns may be seen in the spectra, with weak peaks at around 615 and 1311 cm^{-1} and major peaks at

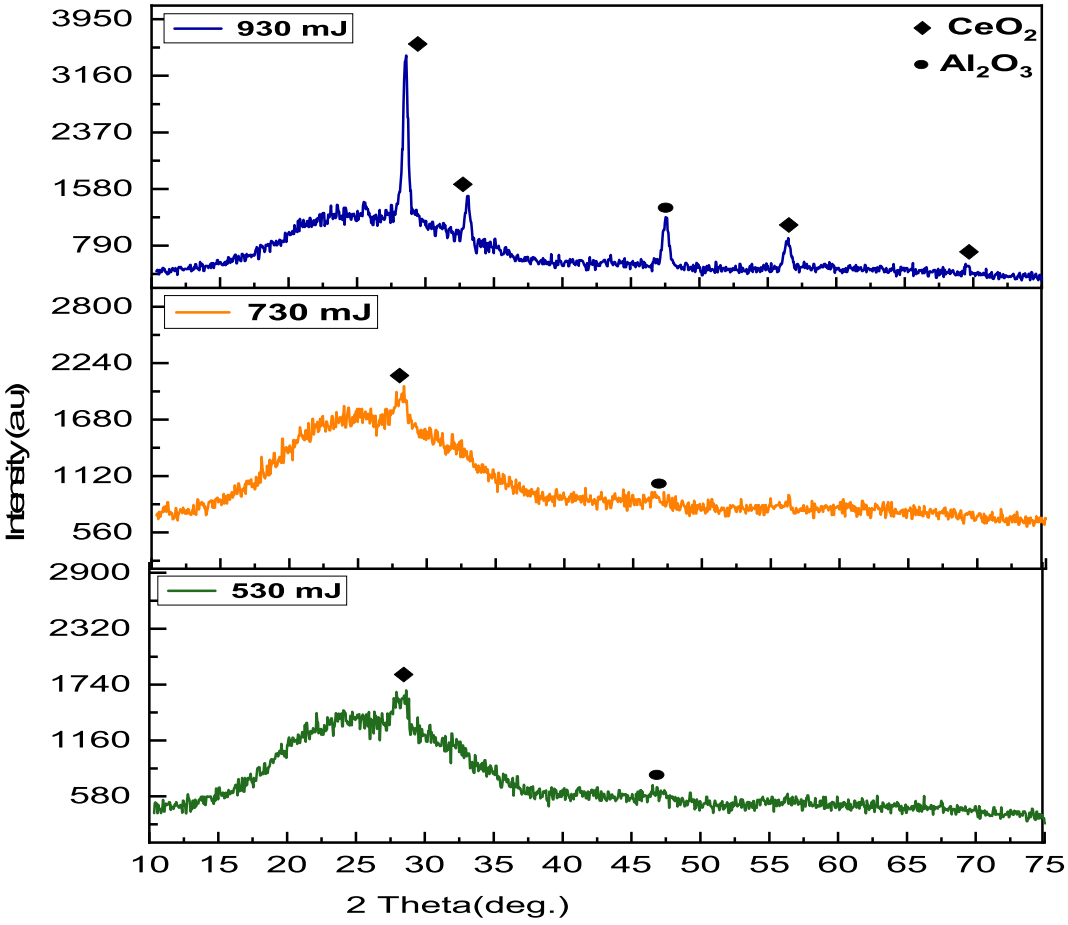

Fig. 2. XRD patterns of CeO_2:Al_2O_3 nano composite at different pulse laser energies.

Table 1. X-ray diffraction peak estimates for CeO_2:Al_2O_3 nanoparticle at different pulse laser energies.

Pulse laser energy mJ	Pos. [°2Th.]	FWHM (Deg.)	d-spacing Exp.(Å)	D (nm)	Phase	hkl
530	28.3700	0.9840	3.14600	8.3	CeO_2 cubic	(111)
	46.8617	2.3616	1.93877	3.7	Al_2O_3 cubic	(400)
730	28.1869	0.7872	3.16602	10.4	CeO_2 cubic	(111)
	46.6590	2.3616	1.94672	3.7	Al_2O_3 cubic	(400)
930	28.5190	0.2952	3.12989	27.8	CeO_2 cubic	(111)
	33.0933	0.2460	2.70698	33.7	CeO_2 cubic	(200)
	47.6117	0.4428	1.90997	19.6	Al_2O_3 cubic	(400)
	56.4248	0.3936	1.63078	22.9	CeO_2 cubic	(311)
	76.9052	0.5904	1.23971	17.2	CeO_2 cubic	(420)

approximately 452, 519, and 979 cm^{-1}, in which its intensity increased as lase energy, the observed increase is reasonable at it likely reflects improvements in crystallinity. These spectra show a high and sharp peak centered at 452 cm^{-1}. This sharp Raman peak corresponds to the F_{2g} Raman vibrational mode of fluorite-type CeO_2, indicating a high degree of crystallinity of cubic symmetry.[24] The peak associated with 519 cm^{-1} is the porous silicon n-type phonon mode.[25] One reason the samples have a big, uneven peak at about 979 cm^{-1} could be the second-order phonon, which relates to local modes around vacancies. Consequently, it is assumed that the CeO_2 samples can function as more effective photocatalysts by preventing electron-hole pair recombination through the addition of oxygen vacancies or by raising the concentration at their surface.[24] The presence of the alpha alumina peak at 1313 cm^{-1} suggests the presence of a very small amount of Al_2O_3, while the weak peak at roughly 615 cm^{-1} belonged to the symmetry A_{1g} vibrational mode of Al_2O_3.[26] The peak 1313 cm^{-1} might be ascribed to the phase transition from theta alumina to alpha alumina when combined with XRD observations. Both visible Raman

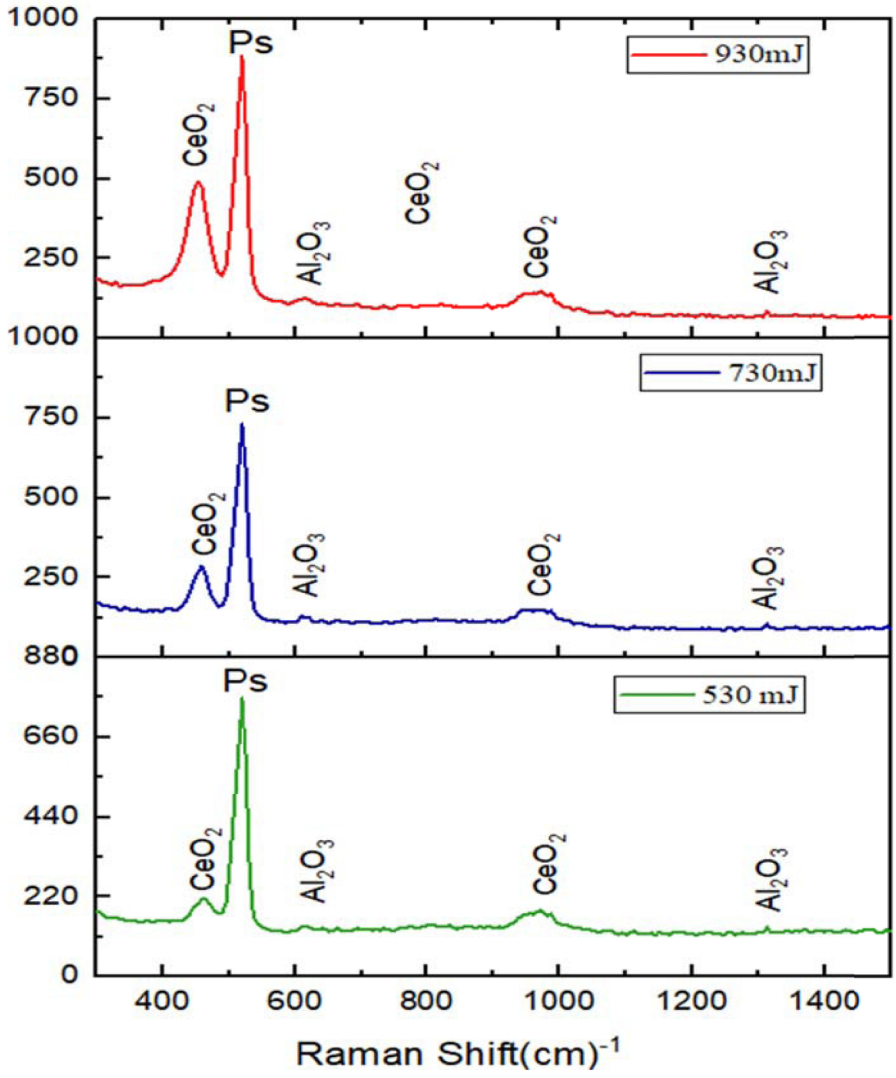

Fig. 3. Raman spectroscopy patterns of CeO_2:Al_2O_3 nanocomposite at different pulse laser energies.

spectroscopy and XRD provide comparable structural information. This might be related to the fact that visible Raman spectroscopy is better at picking up changes in phase than XRD, which needs a long-range order, and that visible Raman spectroscopy is in charge of band change. High-intensity lasers transform theta to alpha alumina.

Atomic force microscopy of CeO_2:Al_2O_3 nanocomposite

Fig. 4 shows the AFM images of the surface of the CeO_2:Al_2O_3 Composite at pulse laser energies of 530, 730, and 930 mJ on the glass substrate. It was observed that the surface morphologies and roughness of CeO_2:Al_2O_3 were obviously different depending on laser energy. The CeO_2:Al_2O_3 particles energy pulse at 530, 730, and 930 mJ show average heights of 18.65, 20.40, and 28.94 nm and Root mean square values of 23.75, 25.12, and 41.75 nm, respectively. The RMS surface roughness rises as laser energy increases.[27] The greater grain size of the CeO_2:Al_2O_3 thin films and the formation of tiny grains with ever bigger sizes and polycrystalline structures are the causes of the increased roughness. According to the AFM pictures, the thin films' surface morphology shows that the grains are dispersed uniformly. Gas sensors and other applications require this surface characteristic.

Field emission scanning electron microscope of CeO_2:Al_2O_3 nanocomposite

The CeO_2:Al_2O_3 Composite deposited on the PS n-type substrate with different Magnifications of 500 nm and 10 μm was investigated by FESEM, as shown in Fig. 5. The majority of the CeO_2 and

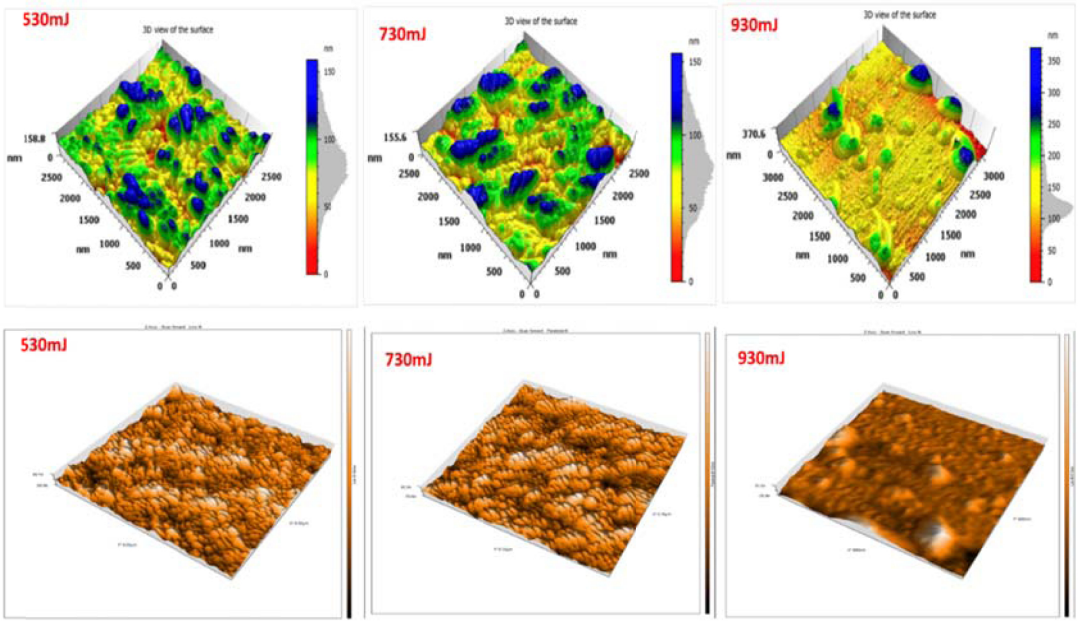

Fig. 4. AFM images of CeO_2:Al_2O_3 nanoparticle at different pulse laser energies.

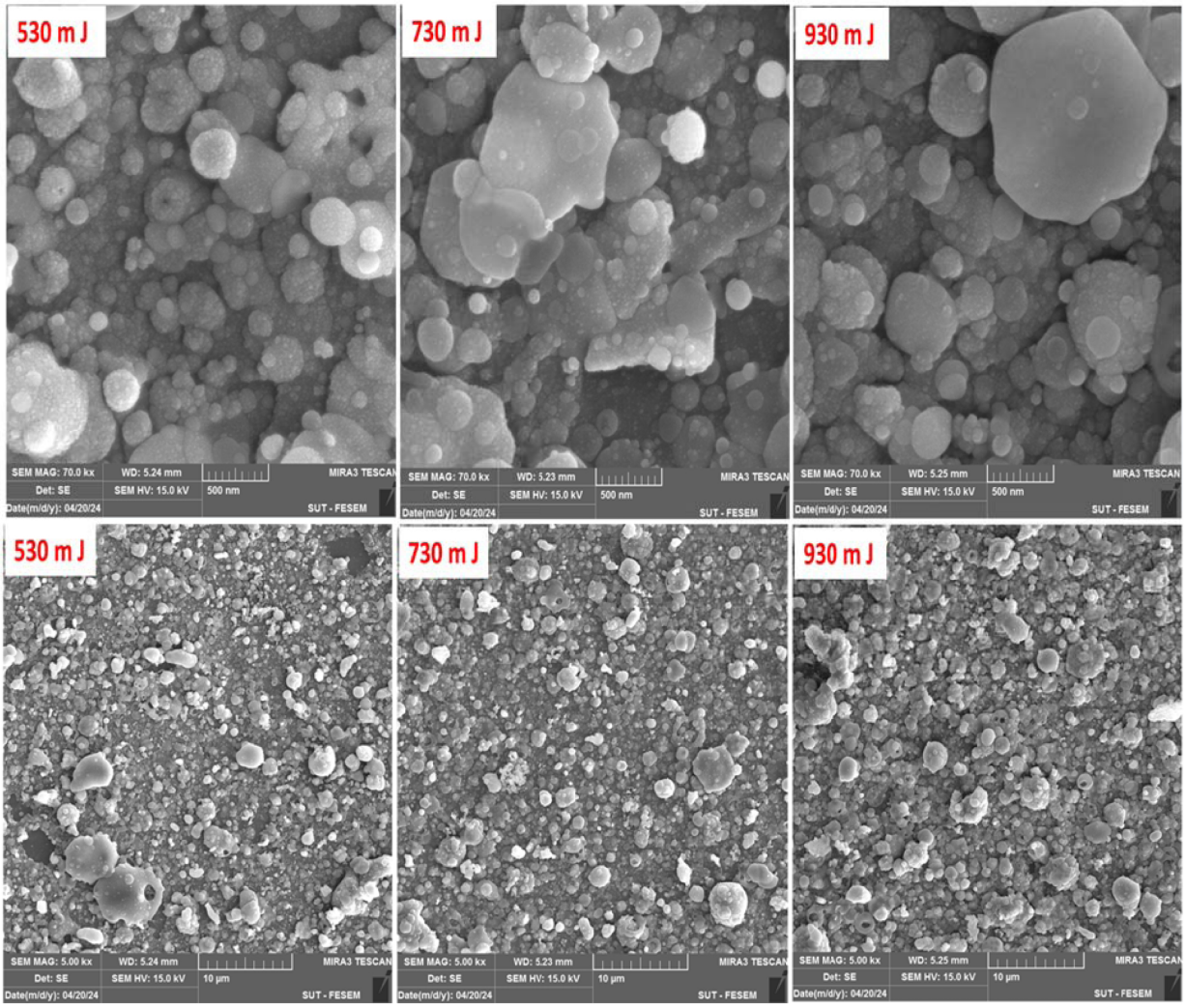

Fig. 5. FESEM images of CeO_2:Al_2O_3 nanocomposite with different Magnifications of 500 nm and 10 μm at different pulse laser energies.

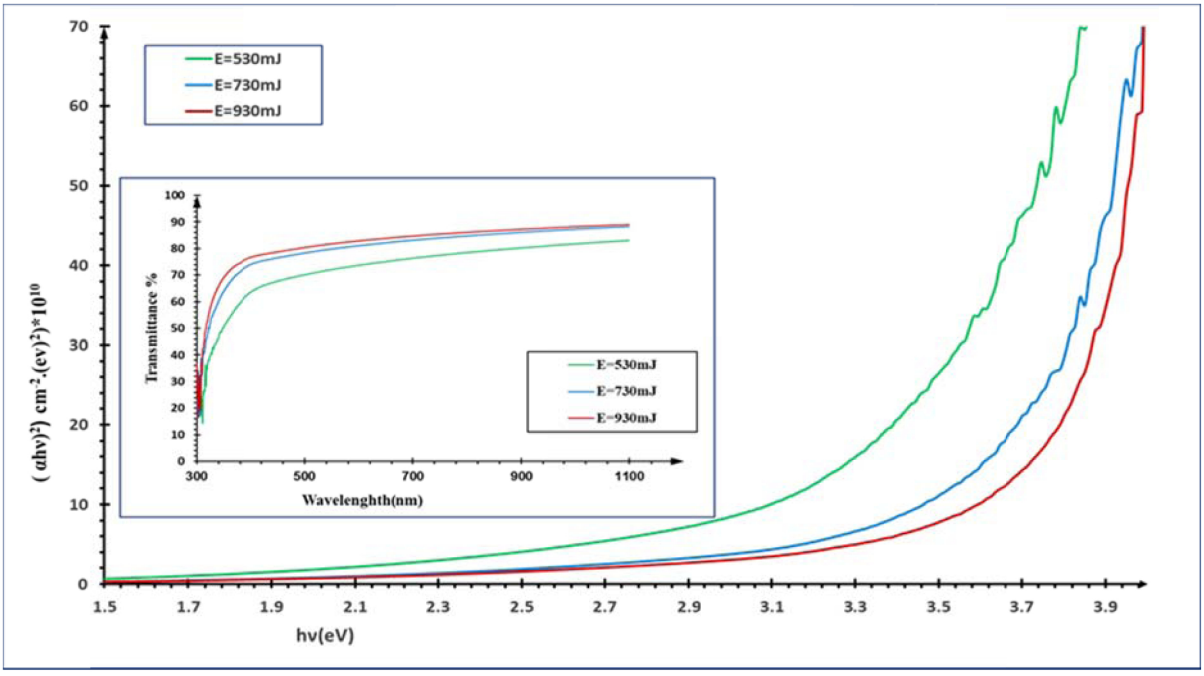

Fig. 6. The hυ versus $(\alpha h\upsilon)^2$ plot of CeO_2:Al_2O_3 composite nanostructures.

Al_2O_3 Particles was found to most have spherical nanostructures, with an average size of (14, 16, 18) nm, respectively with laser energy 530, 730 and 930 nm. There aren't any noticeable variations across the samples, suggesting that each sample's physical makeup is comparable, and agglomerations significantly increase with increasing pulse laser intensity.

UV-V spectroscopy analysis of CeO_2:Al_2O_3 nanocomposite

We studied the optical properties of CeO_2: Al_2O_3 composite nanostructures in the 300–1200 nm range using UV-V spectroscopy. The nanostructures were made using pulse laser deposition (PLD) on glass substrates at room temperature with pulse laser energies 530,730 and 930 mJ. The optical transmittance spectra of the CeO_2: Al_2O_3 nanostructures as a function of wavelength are shown in Fig. 6. It shows up as a broad transmission from the visible to ultraviolet spectra. transmittance in the visible and near infrared region of better than 88% at E= 930mJ, while it was reduced at E=730 and 530 mJ. In solar cell applications, the high transmittance values of CeO_2: Al_2O_3 indicate that the generated samples are best suited for use as a window layer. The optical energy gap for CeO_2: Al_2O_3 nanocomposite has been determined using Eq. (2). These films' band gap may be calculated by extrapolating the straight-line extension of the depicted curve's linear portions to $(\alpha hv)^2 = 0$. The optical bandgap of CeO_2: Al_2O_3 thin films was determined to be 2.36, 2.62, and 2.66 eV for 530 mJ, 730 mJ, and 930 mJ, respectively, at varying laser energies. The quantum confinement effect caused the energy gap to widen as the laser pulse energy grew. Studying the refractive index (n) and the extinction coefficient (k) will complete the basic study of the optical properties and behavior of the nanocomposite. Using a transmittance spectrum, n and k were calculated as a function of wavelength in the 300–1000 nm range by Eqs. (3) and (4). Fig. 7 For CeO_2: Al_2O_3 thin film deposits at room temperature and with different laser energies (530, 730, and 930 mJ), the refractive index and extinction coefficient vary with wavelength. It can be observed that as the wavelength increases, the extinction coefficient increases and the refractive index drops. The growing energy gap impacts the morphology of the films, causing a change in the refractive index. Also, Fig. 7 illustrates that, depending on the concentration rate of mixing materials and the conditions of preparation, the refractive index of approximately 1.7 can be achieved along the visible-NIR region and is suitable for optical filter applications. By optimally choosing the deposition conditions, we successfully control the phenomenon of dispersion, achieving a stable refractive index, which is very important in optical coating applications. [16,17]

Conclusion

Pulsed laser deposition is a simple and highly flexible method for producing thin films and nanomaterials from a wide range of materials. PLD has successfully produced ultra-high-quality

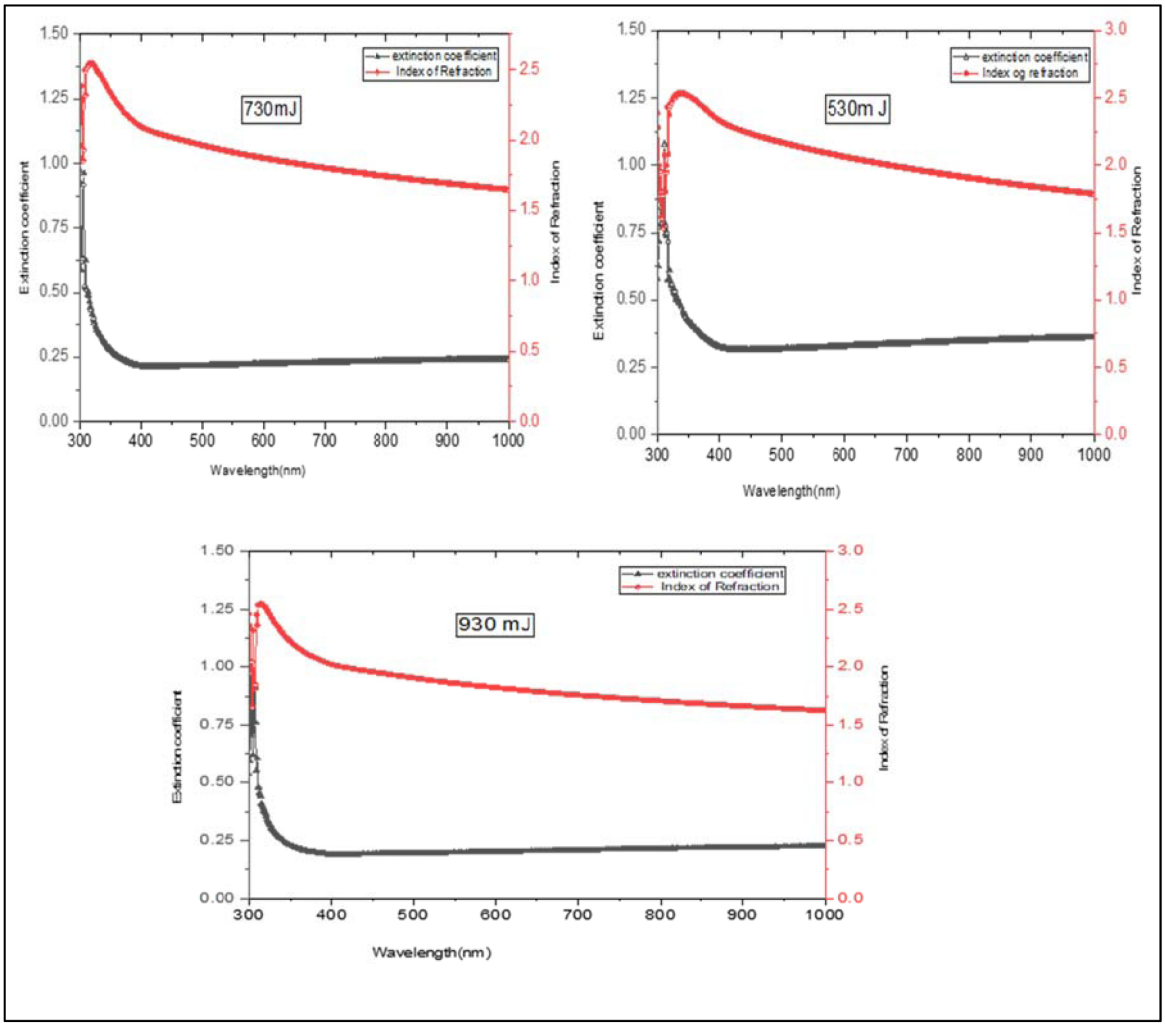

Fig. 7. The refractive index and extinction coefficient of CeO_2:Al_2O_3 composite nanostructures.

crystalline CeO_2:Al_2O_3 nanocomposite thin films on porous N-type silicon substrates. PLD deposits metals not only on the bottom of the pores but also on the walls and openings of the pores, as porous silicon is a porous semiconductor electrode and is therefore used in a variety of optical applications. solar cells, sensors, and optical coatings are proposed as future directions based on the observed material properties such as solar cells, sensors, and optical coatings are proposed as future directions based on the observed material properties. CeO_2:Al_2O_3 nanocomposite thin film structure, morphology, and optical characteristics have all been studied in relation to laser settings (pulse energy), and the use of these materials in a range of applications is affected by this. An aluminum oxide and cerium oxide nanoparticle's XRD results revealed the existence of a polycrystalline cubic phase structure. The findings also showed that the particles that had clumped together crystallized well at 930 mJ laser pulse energies, and the Raman spectra bands were clearer and stronger at that level. The average size and roughness of the irregular nanostructures with varying diameters grew as the laser's energy rose, according to the AFM and FESEM. The CeO_2:Al_2O_3 nanostructures can pass a lot of light, from visible to ultraviolet, up to 88% at E = 930 mJ. They work best for solar cell applications. The quantum confinement effect caused the energy gap to widen as the laser pulse energy grew.

Acknowledgments

We would like to thank the University of Baghdad, College of Science for Women, Department of Physics, Postgraduate Lab. for Medical Physics, for ensuring the availability of all research facilities.

Authors' declaration

- Conflicts of Interest: None.
- We hereby confirm that all the Figures and Tables in the manuscript are ours. Furthermore, any

Figures and images that are not ours have been included with the necessary permission for republication, which is attached to the manuscript.
- No animal studies are present in the manuscript.
- No human studies are present in the manuscript.
- Ethical Clearance: The project was approved by the local ethical committee at the University of Baghdad.

Authors' contributions statement

A. N., N. H., and S.M. conceived and planned the experiments, provided critical feedback, helped in analyzing the data, and reviewed the manuscript.

Data availability

The datasets generated and analyzed during the current study are available from the corresponding author upon reasonable request.

References

1. Abdulrazaq MA, Agava IM, Enejoh OT, Usman MA, AbdulAzeez AA . Effect of mechanical properties of glass fiber reinforced epoxy composites filled with $Al2O_3$ and SiO_2 particles. Inter J Adva Eng Manag. (IJAEM). 2024;6(6):692–698. http://dx.doi.org/10.35629/5252-0606692698.
2. Jaffer ZJ, Mazhir SN, Khalaf MK, Hanon MS. Synthesis and surface characterization of PMMA polymer films in pure oxygen, argon, and nitrogen glow discharge plasma. J Phys: Conf Ser. 2021;1829(1):012010. http://dx.doi.org/10.1088/1742-6596/1829/1/012010.
3. Lunetto V, Galati M, Settineri L, Iuliano L. Sustainability in the manufacturing of composite materials: A literature review and directions for future research. J Manu Proce. 2023;85:858–874. https://doi.org/10.1016/j.jmapro.2022.12.020.
4. Algaffar ANA, Abdalameer NK, Tariq SZ. Laser-ablated SiO_2:TiO_2 plasma optical emission spectroscopy. Inter J Nanos., 2022;21(06):2250049. https://doi.org/10.1142/S0219581X22500491.
5. Abed HA, Al Rashid SNT, Mazhir SN. The optical and structural properties of the Fe@Au core–shell nanoparticles prepared by PLAL. Inter J Nanos., 2023;22(6):2330005. https://doi.org/10.1142/S0219581X23300055
6. Ray SK, Dahal R, Ashie MD, Alonzo SMM, Bastakoti BP. Recent progress on cerium oxide-based nanostructures for energy and environmental applications. Adva En Sust Rese., 2025;2. https://doi.org/10.1002/aesr.202500022.
7. Vangelista S, Piagge R, Ek S, Sarnet T, Martella C, Lamperti A. Structural, chemical and optical properties of cerium dioxide film prepared by atomic layer deposition on TiN and Si substrates. Thin solid films. 2017;636:78–84. https://doi.org/10.1016/j.tsf.2017.05.034.
8. Das HT, Elango BT, Dutta S, Das N, Das P, Mondal A, *et al*, Recent trend of CeO2-based nanocomposites electrode in supercapacitor: A review on energy storage applications, J Energy Storage. 2022;50:104643. https://doi.org/10.1016/j.est.2022.104643.
9. Abdulrahman SA, Ismail RA, Jawad MF. Advancements and challenges in pulsed laser-deposited hydrophobic CeO_2 film for broadband antireflection applications. J Opt. 2024;53(3):2745–2756. https://doi.org/10.1007/s12596-023-01465-7.
10. Ebrahimi P, Kumar A, Khraisheh M. A review of CeO_2 supported catalysts for CO_2 reduction to CO through the reverse water gas shift reaction. Catalysts. 2022;12(10):1101. https://doi.org/10.3390/catal12101101.
11. Singh KR, Nayak V, Sarkar T, Singh RP. Cerium oxide nanoparticles: properties, biosynthesis and biomedical application. RSC Adv. 2020;10(45):27194–27214. https://doi.org/10.1039/d0ra04736h.
12. Yan H, N. Zhang, D. Wang. Highly efficient CeO_2-supported noble-metal catalysts: From single atoms to nanoclusters. Chem Catalysis. 2022;2(7):1594–1623. https://doi.org/10.1016/j.checat.2022.05.001.
13. Balakrishnan G, Babu RV, Shin KS, Song JJ. Growth of highly oriented γ-and α-Al_2O_3 thin films by pulsed laser deposition. Optics Laser Tech. 2014;56:317–321. https://doi.org/10.1016/j.optlastec.2013.08.014.
14. Moodispaw MP, Cinkilic E, Miao J & Luo AA. The beneficial effect of iron in aluminum-cerium-based cast alloys. Metall Mater Trans A. 2024;55:1351–1362. https://doi.org/10.1007/s11661-024-07333-8.
15. Abd Algaffar AN, Ali Jasem N, Abbo AI. Notch filters design with enhanced performance. J Phys.: Conf Ser. 2019;1178(1):012017. https://doi.org/10.1088/1742-6596/1178/1/012017.
16. Aybike B, Seda A, Yucel Y, Ozgur Pt, Dinara S, Cengiz S, Yasemin C, Mujdat C. Structural and optical evolution in CeO2 films induced by aluminum doping: A comprehensive study. Ceram Int. 2025;51(3):2846–2860, https://doi.org/10.1016/j.ceramint.2024.11.262.
17. Ferreira MP, Martínez-Martínez D, Chemin JB, Choquet P. Tuning the characteristics of Al2O3 thin films using different pulse configurations: Mid-frequency, high-power impulse magnetron sputtering, and their combination. Surface Coat Techn. 2023;466:129648. https://doi.org/10.1016/j.surfcoat.2023.129648.
18. Wei Z, Fangling M, Xiaoman L, Zhen L, Xuerui P, Zhen Y, Yanlei L, Zhiqiang Z, Bao L, Nian C, Zhenyu X. Sputtering Al2O3 as an effective interface layer to improve open-circuit voltage and device performance of Sb2Se3 thin-film solar cells. Mater Scie Semico Proce. 2023;153:107185. https://doi.org/10.1016/j.mssp.2022.107185.
19. Jiang M, Wang B, Yao Y, Li Z, Ma X, Qin S, Sun Q. A comparative study of CeO2-Al2O3 support prepared with different methods and its application on MoO3/CeO2-Al2O3 catalyst for sulfur-resistant methanation. Appl Surf Sci. 2013;285:267–277. https://doi.org/10.1016/j.apsusc.2013.08.049.
20. Al Farraj DA, Al-Mohaimeed AM, Alkufeidy RM, N. A. Alkubaisi. Facile synthesis and characterization of CeO2-Al2O3 nano-heterostructure for enhanced visible-light photocatalysis and bactericidal applications. Colloid Inter Sci Comm. 2021;41:100375. https://doi.org/10.1016/j.colcom.2021.100375.
21. Harb NH. Preparation and characterization of NiONPS sensor prepared by different Q-switched Nd: YAG laser parameter: energy pulse and wavelength. Baghdad Sci J. 2025;22. https://doi.org/10.21123/bsj.2024.9984.
22. Harb NH, Twafeeq MT, Abbas AA, Mutlak FA. Laser-ablative synthesis of aqueous solutions of transparent conducting oxide nanoparticles for optoelectronic applications. J Opt. 2024;1–11. https://doi.org/10.1007/s12596-024-02186-1.

23. Balakrishnan G, Venkatesh BR, Shin KS, Song JI. Growth of highly oriented γ-and α-Al2O3 thin films by pulsed laser deposition. Optics Laser Techn. 2014;56:317–321. https://doi.org/10.1016/j.optlastec.2013.08.014.
24. Gong J, Meng F, Fan Z, Li H, Du Z. Template-free controlled hydrothermal synthesis for monodisperse flowerlike porous CeO2 microspheres and their superior catalytic reduction of NO with NH3. J Alloys Comp. 2017;690:677–687. http://dx.doi.org/10.1016/j.jallcom.2016.08.183.
25. Weiwei Z, Baosong L, Ming H, Mingyuan L. Effects of cerium oxide doping on microstructure and properties of Ni-GO-CeO2 nanocomposite coatings. J Mater Rese Techno. 2022;21:3440–3450, https://doi.org/10.1016/j.jmrt.2022.10.149.
26. Junhui L, Guojie C, Nafees A, Muhammad I, Shuo C, Zhenghua S, *et al.* Back contact interfacial modification mechanism in highly-efficient antimony selenide thin-film solar cells. J Energy Chem. 2023;80:256–264. https://doi.org/10.1016/j.jechem.2023.01.049.
27. Zhao X, Li K, Chen Z, Dellith J, Dellith A, Diegel M, Blaschke D, Menzel S, Polian I, Schmid H, Du N. Impact of laser energy density on engineering resistive switching dynamics in self-rectifying analog memristors based on BiFeO3 thin films. J Appl Phys. 2024;135(13):135303. https://doi.org/10.1063/5.0196718.

اطياف رامان والخصائص البصرية لأكاسيد المركبات النانوية السيريوم: الألومنيوم المحظرة بتقنية الترسيب بالليزر النبضي

الاء نزار عبدالغفار، نهى حسن حرب، صباح نوري مزهر

قسم الفيزياء، كلية العلوم للبنات، جامعة بغداد، بغداد، العراق.

الخلاصة

بحثت هذه الدراسة في تأثيرات طاقة الليزر على آلية تغير الطور، والخصائص البصرية، وبنية مركبات نانوية من CeO2:Al2O3المحضرة بتقنية ترسيب بالليزر النبضي (PLD). أُجريت الدراسة باستخدام مطيافية رامان، ومطيافية الأشعة فوق البنفسجية والمرئية(UV-Vis)، وحيود الأشعة السينية (XRD)، ومجهر القوة الذرية (AFM)، والمجهر إلكتروني الماسح (FESEM). وتم المقارنة بين النتائج باستخدام شدات ليزر نبضي مختلفة (530، و730، و930 ملي جول). أُنشئت ركائز سيليكون مسامية (PS) باستخدام النقش الكهروضوئي الكيميائي للسيليكون من النوع n. أظهرت نتائج حيود الأشعة السينية لجسيمات CeO2:Al2O3 النانوية وجود بنية طور مكعب متعدد البلورات. كشف مطياف رامان لمركبات CeO_2:Al_2O_2 عن قيم ضعيفة عند حوالي 615 و1311 سم$^{-1}$، واقمم رئيسية عند حوالي 452 و519 و979 سم$^{-1}$، مع تزداید شدتها مع زيادة طاقة الليزر. ترتفع خشونة سطح RMS بزيادة طاقة الليزر. تتميز غالبية المركبات النانوية بهياكل نانوية كروية موزعة عشوائيًا وتزداد بشكل أكبر عند زيادة طاقة الليزر. تم تحديد فجوة النطاق الضوئية للأغشية الرقيقة CeO_2: Al2O3 لتكون 2.36 و2.62 و2.66 إلكترون فولت لطاقات الليزر المتغيرة. تسبب تأثير التقيد الكمي في اتساع فجوة الطاقة مع نمو طاقة نبضة الليزر. يُسهم أكسيد السيريوم بشكل كبير في النتائج، ويُفضّل استخدامه على المواد التقليدية في المركبات النانوية، إذ يُحسّن خصائص المواد الأساسية ويجعلها أكثر استقرارًا عند ترسيبها في درجات حرارة عالية. وهو ما يظهر في هذا العمل. ويُستخدم أيضًا في التطبيقات البصرية ومجموعة متنوعة من التطبيقات الأخرى.

الكلمات المفتاحية: الألومنيوم ، الخصائص البصرية، الترسيب بالليزر النبضي، النقش الكهروكيميائي الضوئي، رامان.